Cold-rolling influence on microstructure and mechanical properties of NiCr - Ag composites and porous NiCr obtained by liquid metal dealloying

Morgane Mokhtari, Christophe Le Bourlot, Jérôme Adrien, Sylvain Dancette, Takeshi Wada, Jannick Duchet-Rumeau, Hidemi Kato, Eric Maire

Accepted Manuscript

Cold-rolling influence on microstructure and mechanical properties of *NiCr-Ag* composites and *porous NiCr* obtained by liquid metal dealloying

Morgane Mokhtari, Christophe Le Bourlot, Jérôme Adrien, Sylvain Dancette, Takeshi Wada, Jannick Duchet-Rumeau, Hidemi Kato, Eric Maire

PII: S0925-8388(16)34023-3

DOI: 10.1016/j.jallcom.2016.12.105

Reference: JALCOM 40027

To appear in: *Journal of Alloys and Compounds*

Received Date: 31 July 2016

Revised Date: 8 November 2016

Accepted Date: 8 December 2016

Please cite this article as: M. Mokhtari, C. Le Bourlot, J. Adrien, S. Dancette, T. Wada, J. Duchet-Rumeau, H. Kato, E. Maire, Cold-rolling influence on microstructure and mechanical properties of *NiCr-Ag* composites and *porous NiCr* obtained by liquid metal dealloying, *Journal of Alloys and Compounds* (2017), doi: 10.1016/j.jallcom.2016.12.105.

Cold-rolling influence on microstructure and mechanical properties of *NiCr-Ag* composites and *porous NiCr* obtained by liquid metal dealloying

Morgane Mokhtari[1,2,3], Christophe Le Bourlot[1], Jérôme Adrien[1], Sylvain Dancette[1], Takeshi Wada[2], Jannick Duchet-Rumeau[3], Hidemi Kato[2], Eric Maire[1]

[1]Univ Lyon, National Institute of Applied Science of Lyon, MATEIS Laboratory, Villeurbanne, France
[2]Institute for Materials Research, Tohoku University, Katahira, Sendai 980-8577, Japan
[3] Univ Lyon, National Institute of Applied Science of Lyon, IMP Laboratory, Villeurbanne, France
Corresponding author: christophe.le-bourlot@insa-lyon.fr

Abstract

To obtain anisotropic nanoporous *NiCr*, some *NiCr-Ag* composites were prepared using a liquid metal dealloying method and were cold rolled before etching. While immersing $(Ni_{90}Cr_{10})_{60}Cu_{40}$ precursors in a molten *Ag* bath, *Cu* atoms selectively migrate into the *Ag* bath. After cooling down to room temperature, the resulting microstructure is a bi-continuous structure of *NiCr* and A*g* (with *Cu* in solid solution). These ingots are strong enough to be cold rolled in one or two (perpendicular) directions with a thickness reduction of 70%. A final etching step removes the A*g* solid-state solution phase. The influence of cold rolling on the microstructure was investigated using X-ray tomography and on the mechanical properties using nanoindentation. We will show how introducing anisotropy into the microstructure and in the mechanical properties was successful while being able to preserve the porous state.

Keywords

dealloying, X-ray tomography, nanoindentation, Ni, cold rolling, porous

Highlights

→ *NiCr-Ag* composites were prepared by dealloying *Ni-Cr-Cu* precursor in an *Ag* melt bath
→ *NiCr-Ag* composites were cold-rolled to introduce anisotropy
→ The microstructure of *NiCr-Ag* and porous *NiC*r composites was studied using X-ray tomography
→ The mechanical properties of *NiCr-Ag* and porous *NiCr* composites were examined by nanoindentation

1. Introduction

Nanoporous metals have attracted considerable attention for their excellent functional properties [1-4]. Properties at the nanoscale differ significantly from those of their dense, bulky counterparts. The earlier and most well-known technique used to prepare such nanoporous metals is dealloying in aqueous solution. Nanoporous noble metals including *Au, Ag, Pt, Pd* and *Cu* have been successfully prepared from binary alloy precursors such as *Au-Ag*, *Ag-Al*, *Pt–Cu*,

Pd–Co, *Cu–Mn* and *Cu-Al* [4-10]. Regarding less noble metals, unstable in aqueous solution, the previous process is impossible as they oxidize immediately when coming into contact with water. To overcome this limitation, a new dealloying method using a metallic melt instead of aqueous solution was recently developed [11]. The liquid metal dealloying method is a selective dissolution phenomenon of a bi-alloy solid precursor: one component (referred to as the soluble component) being soluble in the metallic melt while the other (referred to as the targeted component) is not. When the solid precursor is immersed in the metallic melt, only atoms of the soluble component dissolve into the melt inducing a spontaneously organized bi-continuous microstructure formed by the targeted and sacrificial phases (the atoms of the sacrificial phase in solution in the melt phase). After cooling down to room temperature, this sacrificial phase can be removed by selective chemical etching to obtain the final nanoporous materials with the targeted composition. Because this is a water-free process, it has enabled the preparation of nanoporous structures with less noble elements such as pure *Ti*, *Fe*, *Cr*, *Nb*, *Si* and *C* [11-17].

In some applications such as electron or heat transportation, great strength along a particular may be desired thus leading to anisotropy in the structure and subsequently in the electrical, thermal or mechanical properties. However no practical methods have thus far been suggested to induce such an anisotropy [21].

The study of the microstructure of these porous materials is not easy because it requires 3D information. The relationship between the microstructure and the mechanical properties of these materials made by liquid metal dealloying has also not yet been clarified.

Nanoporous *Ni*, already prepared by dealloying from *Ni-Mn*, *Ni-Cu*, *Ni-Al* [18-20] in aqueous solution, is directly obtained as a foam. It is therefore not possible to introduce anisotropy after employing a dealloying process such as this. In the present study, we prepare $Ni_{90}Cr_{10}$ with the liquid metal dealloying method using an *Ag* bath. The possibility of introducing anisotropy in the microstructure by cold rolling the dealloyed material before etching the sacrificial phase is studied. The microstructure of the obtained samples is determined using 3D XRCT and its morphological characteristics are quantified. This is linked to the measurement of the mechanical properties of the *NiCr-Ag* composite and (in one case only) of the porous material.

2. Materials and methods

The elements selection strategy for designing the dealloying reaction is based on the interaction (enthalpy of mixing) between atoms, which is described in detail in [11]. A *Ni–Cr–Cu* alloy (the precursor) and an *Ag* melt were used in this work. $(Ni_{90}Cr_{10})_{60}Cu_{40}$ ingots were prepared using arc melting and tilt casting, as described in [14]. The resulting cylinder was cut

into slices 1cm in diameter and 1mm thick. The dealloying step was carried out on these slices with a temperature of 1293K for 30min in an *Ag* melt bath. Before selective etching some dealloyed metallic composite samples were cold-rolled to introduce morphological anisotropy by co-deformation. Three sets of samples were prepared: (i) Non-rolled samples (NR), (ii) samples rolled in one direction (1D) and (iii) samples rolled in two perpendicular directions (2D); the cold-rolling process was performed with a 70% reduction in thickness. The selective etching step was carried out using highly concentrated nitric acid to dissolve the solid-state solution of *Ag*, resulting in micro- to nano-porous $Ni_{90}Cr_{10}$.

Each of the composite samples was cut with a precision micro-cutting machine into a rectangular rod with 0.5–1 mm sides and 1 cm in length and then polished into a tip shape for X-ray tomography measurement conducted on a *easytom tomograph* (RX Solutions, France). The polychromatic X-ray source was operated with a LaB_6 cathode at a voltage of 100 kV. The 488 X-Ray projections were collected on a flat panel detector with an exposure time of 10s. The reconstructed 3D images were obtained using the commercial software provided with the tomograph. The full volumes were reconstructed with a voxel lateral isotropic size of 0.3µm and analyzed with Fiji free software [22]. The "*local thickness*" function was used to calculate the phase thickness distribution of each phase. The "*find connected area*" and a homemade plugin were used to measure the connectivity and the specific surface (the surface being approximated using the marching cube algorithm).

Nanoindentation tests were performed using a Nanoindenter G200 device. On each sample 9 indents were performed with (1)a maximum depth of 2µm using a Berkovich diamond tip on composite samples and (ii)a maximum load of 150mN applied in 5 steps with a 70µm diameter cylindrical steel flat punch on porous samples.

The results were analyzed with the Nanosuite software and were calibrated with a fused silica sample. In order to detect a possible mechanical anisotropy induced by rolling, indentation was performed perpendicular to the thickness and along the thickness of the samples.

3. Results and discussion

3.1 Microstructural characterization of *NiCr-Ag* composites

3. 1. 1 Qualitative images

Fig. 1 shows one reconstructed slice for each sample extracted from the reconstruction and the associated threshold outline used for the analysis. The quality of these pictures is affected by the fact that *Ag* and *Ni* are high X-ray absorbing elements, implying the use of high energy X-rays. In such conditions, image quality is not at its best on a standard laboratory tomograph. Note also that despite the fact that we used one of the smallest possible source sizes

available on the market for such a laboratory device, the size of the microstructure of our samples is so small that the resolution is barely enough for a perfect analysis. Despite these remarks, a number of comments can be made. The two phases are clearly visible in Fig. 1. The lighter phase corresponds to the *Ag* phase while the darker one corresponds to the *NiCr* phase. **Fig. 1(a)** shows quite randomly oriented ligaments while **Fig. 1(b)** and **(c)** show ligaments oriented in one direction and **(c)** is more oriented than **(b)**. This is consistent with the imposed cold rolling process, the amount of anisotropy in the 1D sample (along its rolling direction) being expected to be higher than in the 2D sample.

3. 1. 2 Volume fraction and phases thickness

Tomography analysis gives access to the volumic fraction (*%vol*) of the different components while atomic ratios are given by the stoichiometry of the design precursor.

Table 1 shows the measure of the %vol of the *NiCr* phase ratio. The %at amount of *NiCr* included in the precursor was 60%. The %vol is directly extracted from the thresholded images. Given the bad quality of these images, the precision of the measurement is not very good (estimated to about +/- 2%). All ratios measured are rather close to 60 %, which also validate the measurement process (as cold rolling does not affect volume fractions). **Fig. 2(a)** exhibits the phase thickness distributions of *NiCr* and *Ag* phases for the non-rolled sample. As already mentioned in literature for a similar process [23], the phases display a unimodal thickness distribution. The average phase thickness is around 4 µm for the *NiCr* and 5µm for the *Ag*. **Fig. 2(b)** and **(c)** show the influence of cold rolling on the phase thickness distribution respectively for *NiCr* and *Ag* phases. **Fig. 2(b)** presents an almost constant *NiCr* phase average thickness with a slightly wider distribution for cold-rolled samples. **Fig. 2(c)** seems to exhibit a small effect of cold rolling on the *Ag* phase: the isotropic sample presents a smaller average phase thickness than cold-rolled ones. Further investigations are needed to better understand this result, the quality of the raw images prevents any graphical explanations from being given.

3. 1. 3 Connectivity and specific surface

For various applications where the transport of electrical charges is a key property (such as capacitors), it is important to have a perfectly connected structure and a high specific surface [1-4]. The connectivity for all samples is close to 1 for both phases. This result shows that our sample made by dealloying is a bi-continuous structure as mentioned in Wada *et al*. [11]. We then demonstrate here that the cold rolling process does not break the ligaments and that the bi-continuous structure is preserved.

Table 2 gives the specific surface of the samples, bulk *NiCr* density was calculated with atomic fraction and density found in literature [24]. Both the *NiCr* and *Ag* phases have the same volumic specific surface. The specific surface is slightly decreases with cold rolling. The measured values are rather low compared to the *Ni* based alloy made by dealloying in aqueous solution (about twice as high) but our ligament size is about 400 times higher [25]. Nanoporous Au from a 15nm to 70nm ligament size and low density give a specific surface of around 72 10^4 m^2/kg that is higher than our samples but with smaller ligament sizes [26]. For a material elaborated by dealloying, our specific surface is low but still higher than macroporous *Ni* [25, 27]. For this set of samples, we did not particularly target small ligament sizes but this would be perfectly feasible using this dealloying process. A decreasing phase ratio, dealloying time or dealloying temperature will give smaller ligaments and therefore a higher specific surface.

3. 2 Mechanical characterization of *NiCr-Ag* composites

Fig. 3(a) shows load-displacement curves registered during nanoindentation experiments. These curves are rather typical of bulk materials [28] and are similar for each indent, highlighting the reproducibility of the measurement. The maximum indentation depth of 2µm is smaller than the ligament thickness (4µm) but the interaction area should be considered as 10 times the indentation depth so it is considered to be large enough for sampling a representative part of the sample [29]. Oliver *et al* explain how the Young's modulus could be extracted from such load-displacement curves [28]

Fig. 3(b) shows the evolution of the Young's modulus measured along thickness *vs* the perpendicular modulus for different cold rolling conditions. The dashed line corresponds to equality between the two (expected for an isotropic sample). Theoretical *Ag* and *Ni* values from literature are also plotted [24]. Because of the small amount of *Cr* in the *NiCr* phase and because the *Ni* and *Cr* Young's moduli are close to each other, we assumed that the Young's modulus of the *NiC*r phase could be assimilated to that of *Ni* [24]. All *NiCr-Ag* measured moduli are between 130 and 180 GPa, higher than *Ag* but lower than *Ni.* Moreover, the values are closer to *Ni* than to *Ag*, which is consistent with the phase fractions. Dispersion of the nanoindentation results is shown by error lines. The dispersion is small, around 6 GPa, and almost constant, which is consistent with the similar load-displacement curves showed in **Fig. 3(a)**. The NR sample exhibits very similar indents independently of the tested direction while 1D and 2D cold-rolled samples present higher moduli values on the sample thickness than on the sample surface. This confirms that cold rolling indeed induces a mechanical anisotropy, and that the quantity of anisotropy can be controlled by the cold rolling step. Further analyses are needed to quantify this process.

3. 3 Dissolution of NiCr-Ag 1D

3. 3. 1 Microstructural characterization

On *NiCr-Cu* precursor alloy, some SEM-EDX measurement were done, SEM-EDX maps show an homogeneous monophase alloy. **Fig. 4** shows a comparison of an *NiCr-Ag* before and after the chemical etching of the Ag phase. SEM-EDX analysis on the two phases (**Fig. 4(a)**) confirms an clear separation between the phases, with no silver within the *NiCr* phase, and vice versa. After chemical etching (**Fig. 4(b)**), the silver phase has been removed, and a surface average of the SEM-EDX analysis shows no trace of residual silver. Finally, the size and morphology of the foam ligaments after dissolution seem consistent with what is visible before dissolution, because the addition of Chromium in the Nickel create a passivated layer that protect the phase.

Fig. 5 shows one reconstructed slice for each sample extracted from the reconstruction with **(a)** the composite sample also shown in **Fig. 1(c)**, **Fig. 5(b)** and **(d)** display the same sample after 15min immersed in nitric acid and **(c)** after 30min in nitric acid respectively. In **Fig 5(c)**, the sample is nearly completely porous, some white points could be noticed, perhaps due to some residual sacrificial phase. As mentioned for the *Au* sample, the propagation of the dissolution front appears to be planar from outside to inside and the propagation of nitric acid looks faster at the tip than at the side of the sample [29]. Because of the different thermal expansion coefficient between the two phases we can expect some residual thermal-stress between the two phases. The dissolution of the sacrificial phase would therefore relax this stress, even if this relaxation is likely to be small. The image quality is again not good enough to conclude on the tendencies.

3. 3. 2 Mechanical characterization

Table 3 displays the average Young's moduli and standard deviations measured on a composite and porous 1D sample both perpendicular and along the thickness. For the porous sample, the modulus along the thickness (9.8 GPa) is larger than that one measured on the surface (8.1 GPa). This shows the possibility of introducing anisotropy in mechanical properties at the porous state as this anisotropy seems to be preserved after dissolution. To our knowledge, there is no such comparable measurement in literature. For a three-dimensionally ordered macroporous (3DOM) nickel, with smaller pore (1.2µm), smaller ligaments size and lower density (0.26), Young's moduli measured by nanoindentation were 2GPa [30]. This seems rather consistent with the 9 GPa measured on our denser Ni foam.

Gibson and Ashby proposed the equation (1) to link the Young's modulus (E_p) and density (ρ_p) of a porous material with the modulus (E) and density (ρ) of its bulk constituent. C and n are constant values [31].

$$\frac{E_p}{E} = \frac{C * \rho_p^n}{\rho^n} \quad (1)$$

C and n are constant parameters, depending on the morphology of the porous sample [32]. Using C=1 and n=2, as suggested in [32] for open-cell foams, this model predicts E_P=54GPa and E_A=58GPa for the indents perpendicular and along the thickness respectively. This is much larger than our measurements. Molecular dynamic simulations [33] also found that nanoporous gold does not follow the Gibson and Ashby relation and these authors proposed a new model described in equation (2) with ρ_r as the porous to bulk density ratio, and B and D are constants calculated from their data.

$$\frac{E_p}{E} = B * \left(\rho_r^2 + D * \rho_r\right) (2)$$

When applying the B and D values suggested in [33], moduli become E_P=18 and E_A=20 GPa, perpendicular and along the thickness, which is in better agreement with our measurements.

4. Conclusion

NiCr-Ag composites were prepared using dealloying by immersing *Ni-Cr-Cu* precursors into a *Ag* metallic melt bath. One sample was cold-rolled in one direction, another in two perpendicular directions with a thickness reduction of 70% and one was non-rolled. The *Ag* phase of the one direction cold-rolled sample was then etched. The results of X-ray tomography show that the %at fraction of the precursor will determine the %vol faction of the bi-continuous structure. The *NiCr* and *Ag* particle size distribution were independent to cold rolling conditions. The material remains bi-continuous although the cold rolling process indicates a mechanical anisotropy. *NiCr-Ag* composites present Young's modulus values between those expected for *Ni* and *Ag*. Indentations perpendicular to the thickness and along the thickness give similar moduli for the non-cold rolled sample, but is different for those which are cold-rolled. The difference in Young's moduli is measured to be preserved at the porous state after etching. The introduction of anisotropy into the microstructure and the mechanical properties of the composites was well preserved after etching at the porous state.

Acknowledgements

The authors gratefully acknowledge the French ministry of research for the provision of the salary grant of MM.

References

[1] J. *Erlebacher*, R.*Seshadri*, Hard materials with tunable porosity, *MRS Bull 34* (2009) *561*–568

[2] J. Snyder, T. Fujita, M. Chen, J. Erlebacher,Oxygen reduction in nanoporous metal–ionic liquid composite electrocatalysts, Nat. Mater. 9 (2010) 904-907

[3] X.Y. Lang, A. Hirata, T. Fujita, M. Chen,Nanoporous metal/oxide hybrid electrodes for electrochemical supercapacitors, Nat. Nanotechnol. 6 (2011) 232-236

[4] L.Y. Chen, J.S. Yu, T. Fujita, M. Chen, Nanoporous copper with tunable nanoporosity for SERS applications, Adv. Funct. Mater. 19 (2009) 1221–1226

[4] L.Y. Chen, J.S. Yu, T. Fujita, M. Chen, Nanoporous copper with tunable nanoporosity for SERS applications, Adv. Funct. Mater. 19 (2009) 1221–1226

[5] A.J. Forty, Corrosion micromorphology of noble metal alloys and depletion gilding, Nat. 282 (1979) 597-598

[6] C. Xu, Y. Li, F. Tian, Y. Din, Dealloying to nanoporous silver and its implementation as a template material for construction of nanotubular mesoporous bimetallic nanostructures, Chem. Phys. Chem.11 (2010) 3320–3328

[7] D.V. Pugh, A. Dursun, S.G. Corcoran, Formation of nanoporous platinum by selective dissolution of Cu from Cu0.75Pt0.25, J. Mater. Res. 18 (2003) 216–221

[8] U.S Min, J.C.M Li, The microstructure and dealloying kinetics of a Cu-Mn alloy, J. Mater. Res. 11 (1994) 2878–2883

[9] J.R. Hayes, A.M. Hodge, J. Biener, A.V. Hamza, K. Sieradzki, Monolithic nanoporous copper by dealloying Mn–Cu, J. Mater. Res. 21 (2006) 2611-2616

[10] A.J. Smith, T. Tran, M.S. Wainwright, Kinetics and mechanism of the preparation of Raney® copper, J. Appl. Electrochem. 29 (1999) 1085–1094

[11] T. Wada, K. Yubuta, A. Inoue, H. Kato, Dealloying by metallic melt Mater. Lett. 65 (2011) 1076-1078

[12] T. Wada, A. D. Setyawan, K. Yubuta, H. Kato, Nano- to submicro-porous b-Ti alloy prepared from dealloying in a metallic melt, Scr. Mater. 65 (2011), 532-535

[13] Y.-C. K. Chen-Wiegart, T. Wada, N. Butakov, X. Xiao, F. De Carlo, H. Kato, J. Wang, D. C. Dunand, E. Maire, 3D morphological evolution of porous titanium by x-ray micro- and nano-tomography, J. Mater. Res. 28 (2013) 2444-2452

[14] T. Wada, H. Kato, Three-dimensional open-cell macroporous iron, chromium and ferritic stainless steel, Scr. Mater. 68 (2013) 723-726
[15] J.W. Kim, T. Wada, S.G. Kim, H. Kato, Sub-Micron Porous Niobium Solid Electrolytic Capacitor Prepared by Dealloying in a Metallic Melt, Mater. Lett.116 (2014) 223-226
[16] T. Wada, T. Ichitsubo, K. Yubuta, H. Segawa, H. Yoshida, H. Kato, Bulk-Nanoporous-Silicon Negative Electrode with Extremely High Cyclability for Lithium-Ion Batteries Prepared Using a Top-Down Process, Nano Lett. 14 (2014) 4505-4510
[17] S.G. Yu, K. Yubuta, T. Wada, H. Kato,Three-dimensional bicontinuous porous graphite gerenated in low teperature metallic melt, Carbon 96 (2016) 403-410
[18] M. Hakamada, M. Mabuchi, Preparation of nanoporous Ni and Ni–Cu by dealloying of rolled Ni–Mn and Ni–Cu–Mn alloys, J. Alloy Comp. 7 (2009) 583–587
[19] L. Sun,C.-L. Chien, and P. C. Searson, Fabrication of Nanoporous Nickel by Electrochemical Dealloying, Chem. Mater. 16 (2004) 3125-3129
[20] A.J. Smith, P.R. Munroe, T. Tran, M.S. Wainwright, J. Mater. Sci. 36 (2001) 3519–3524
[21] K. Sivula, R. Zboril, F.L. Formal, R. Robert, A. Weidenkaff, J. Tucek, J. Frydrych, M. Grätzel, Photoelectrochemical water splitting with mesoporous hematite prepared by a solution-based colloidal approach, J. Am. Chem. Soc. 132 (2010) 7436-7444
[22] J. Schindelin, I. Arganda-Carreras, E. Frise et al., *Fiji: an open-source platform for biological-image analysis*, Nat. methods 9 (2012) 676-682
[23] W.B. Liu, S.C. Zhang, N. Li, J.W. Zheng, S.S. An, Y.L. Xing, A general dealloying strategy to nanoporous intermetallics, nanoporous metals with bimodal, and unimodal pore size distributions, Corros. Sci. 58 (2012) 133–138
[24] Metals Handbook, Vol.2 - Properties and Selection: Nonferrous Alloys and Special-Purpose Materials, ASM International 10th Ed. 1990
[25] E. Detsi, J. B. Cook, B. K. Lesel, C. L. Turner, Y.-L. Liang, S. Robbennolta, S. H. Tolbert, Mesoporous Ni 60 Fe 30Mn10 -alloy based metal/metal oxide composite thick films as highly active and robust oxygen evolution, Energy Environ. Sci. 9 (2016) 540-549
[26] C. Lakshmanan, R.N. Viswanath, S.R. Polaki, R. Rajaraman, S. Dash, A.K. Tyagi, Surface area of nanoporous gold: Effect on temperature, Electrochim. Acta 182 (2015) 565–572
[27] S. Zhu, X. Yang, W. Yang, L. Zhang, J. Wang, M. Huo, Application of Porous Nickel-Coated TiO2 for the Photocatalytic Degradation of Aqueous Quinoline in an Internal Airlift Loop Reactor, Int. J. Environ. Res. Public Health9(2)(2012) 548-563
[28] W.C. Oliver, G.M. Pharr, An improved technique for determining hardness and elastic modulus using load and displacement sensing indentation experiments, J. Mater. Res. 7 (1992) 1564-1583

[29] J. H. Westbrook, H. Conrad, The Science of hardness testing and its research applications, American Society for Metals, 1973

[30] Y.-C. K. Chen-Wiegart, S. Wang, W.-K. Lee, I. McNulty, P. W. Voorhees, D. C. Dunand, In situ imaging of dealloying during nanoporous gold formation by transmission X-ray microscopy, Acta Mater. 61 (2013) 1118–1125

[31] Z. Li, L. Yang, Y. Li, Y. Yang, C. Zhou, Y. Ding, J. Zhao, Y. Li, Effects of pore size on the mechanical properties of three-dimensionally ordered macroporous nickel, Materials & Design,45 (2013)52-55

[32] X.-Y. Sun, G.-K. Xu, X. Li, X.-Q. Feng, H. Gao, Mechanical properties and scaling laws of nanoporous gold, J. appl. Phys., 113 (2013) 023505

[33] L.J. Gibson, M.F. Ashby, Cellular Solids: Structure and Properties, second ed., Cambridge University Press,Cambridge, 1997

Figure caption:

Fig. 1(a) and (d), non-cold-rolled sample, (b) and (e) two direction cold-rolled samples, (c) and (f) one direction cold-rolled sample.
The white lines of (d), (e) and (f) correspond to the outline of the binarised sample used for the analysis.

Table 1 : Volumic NiCr phase fraction measured by XRCT depending of cold-rolling

Fig. 2 (a)Evolution of NiCr and Ag particle size distribution for an NiCrAg cold-rolled sample
(b) Influence of cold rolling on NiCr particle size distribution
(c) Influence of cold rolling on Ag particle size distribution

Table 2 : Evolution of the specific surface depending on cold rolling conditions

Fig. 3 (a) Load-displacement curve
(b) Evolution of indents perpendicular to the surface and indents along the thickness. Young's modulus with cold rolling. Theoretical Young's modulus of Ni and Ag were found in literature [24]

Fig. 4 (a) SEM picture and EDX curves of 1D composite sample before dissolution (a) and after dissolution (b). Red segments correspond to one ligament size.

Fig. 5 (a) 1D composite sample, (b) and (d) 1D half-porous sample (c) 1D porous sample

Table3 : Evolution of the average Young's Modulus and its standard deviation depending on the indents' position : perpendicular to the thickness (P) along the thickness (A) and the state: composite (Co) and porous (Po)

Tables :

Table 1

	NR	1D	2D
Volumic NiCr phase fraction on NiCrAg samples	0.59	0.61	0.57

Table 2

	NR	2D	1D
Specific surface (m^2/kg)	71	53	65
Specific surface (m^2/m^3)	37 104	30 104	33 104

Table 3:

	P-Co	P-Po	A-Co	A-Po
Average Young's modulus (GPa)	151	8.1	160	9.8
Standard deviation (GPa)	3.1	0.6	3.2	1.8

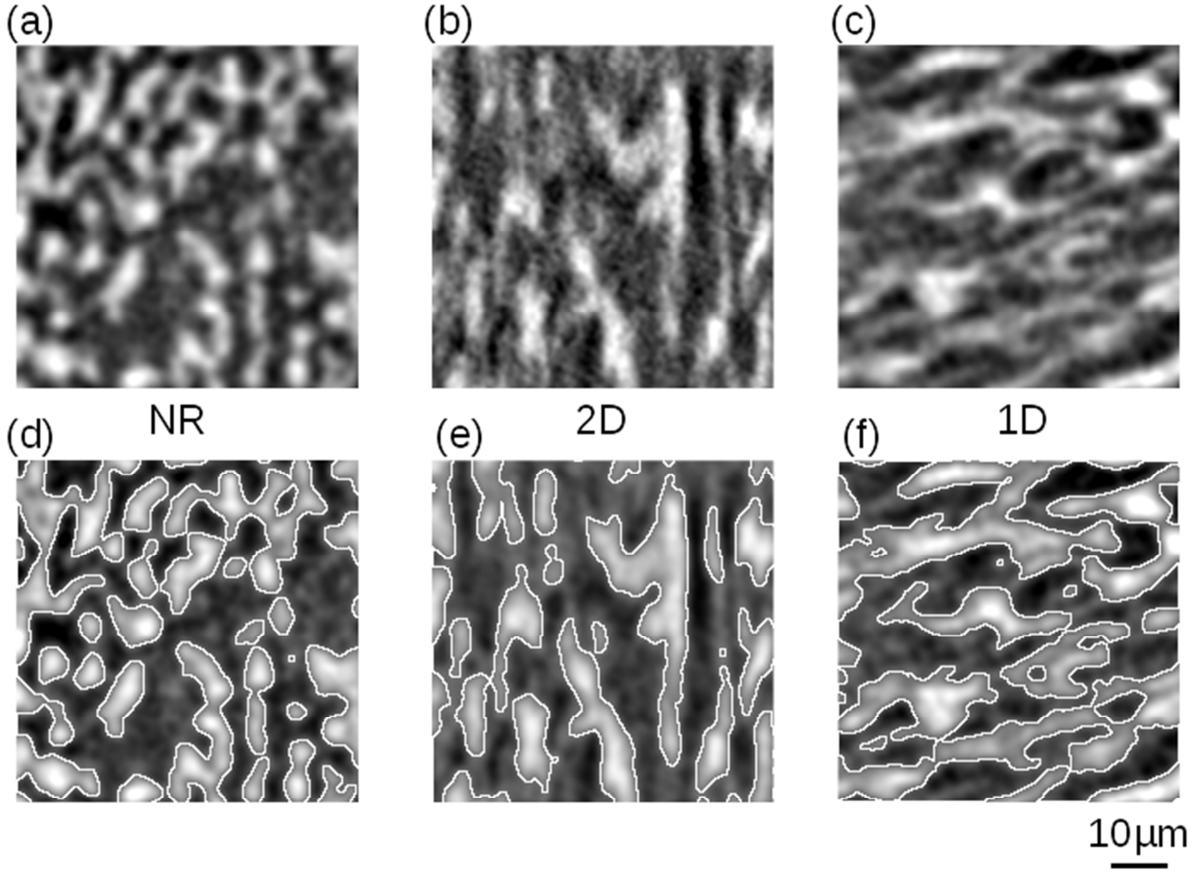

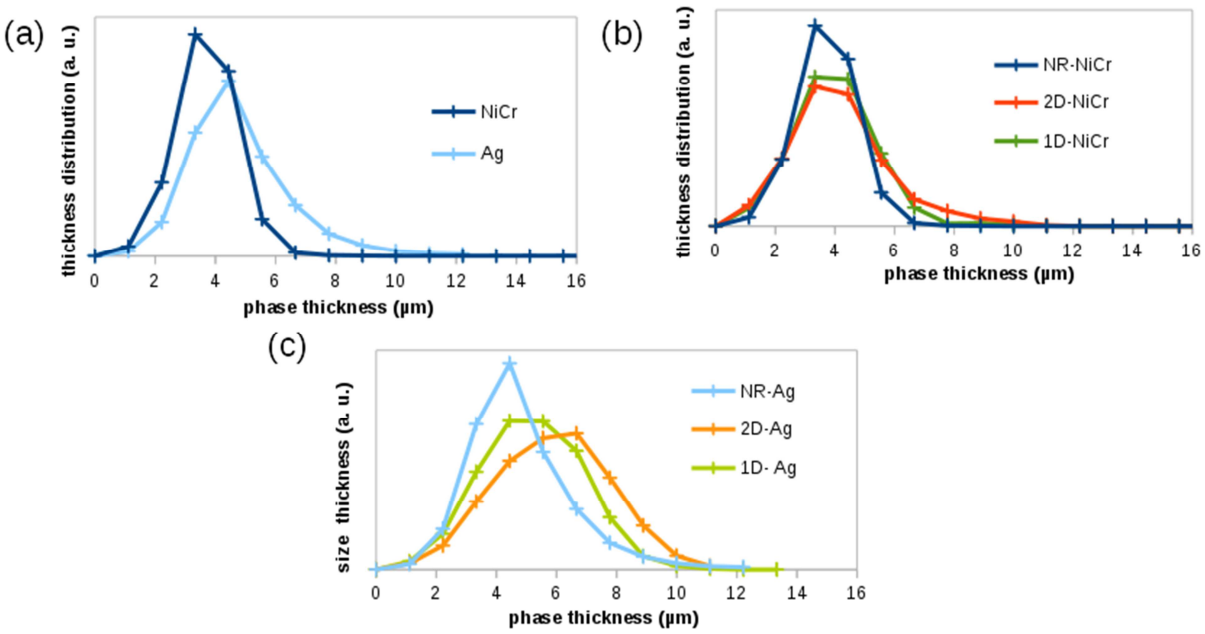

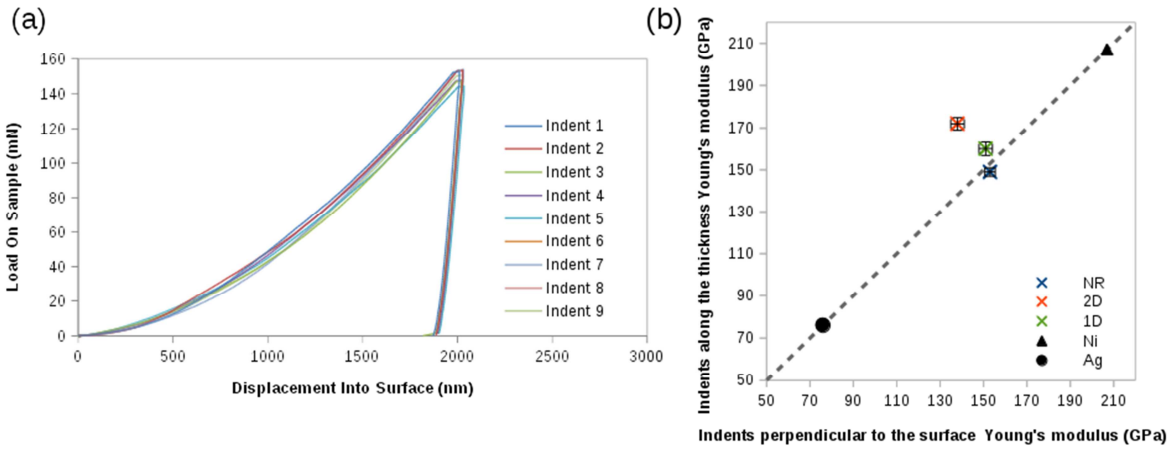

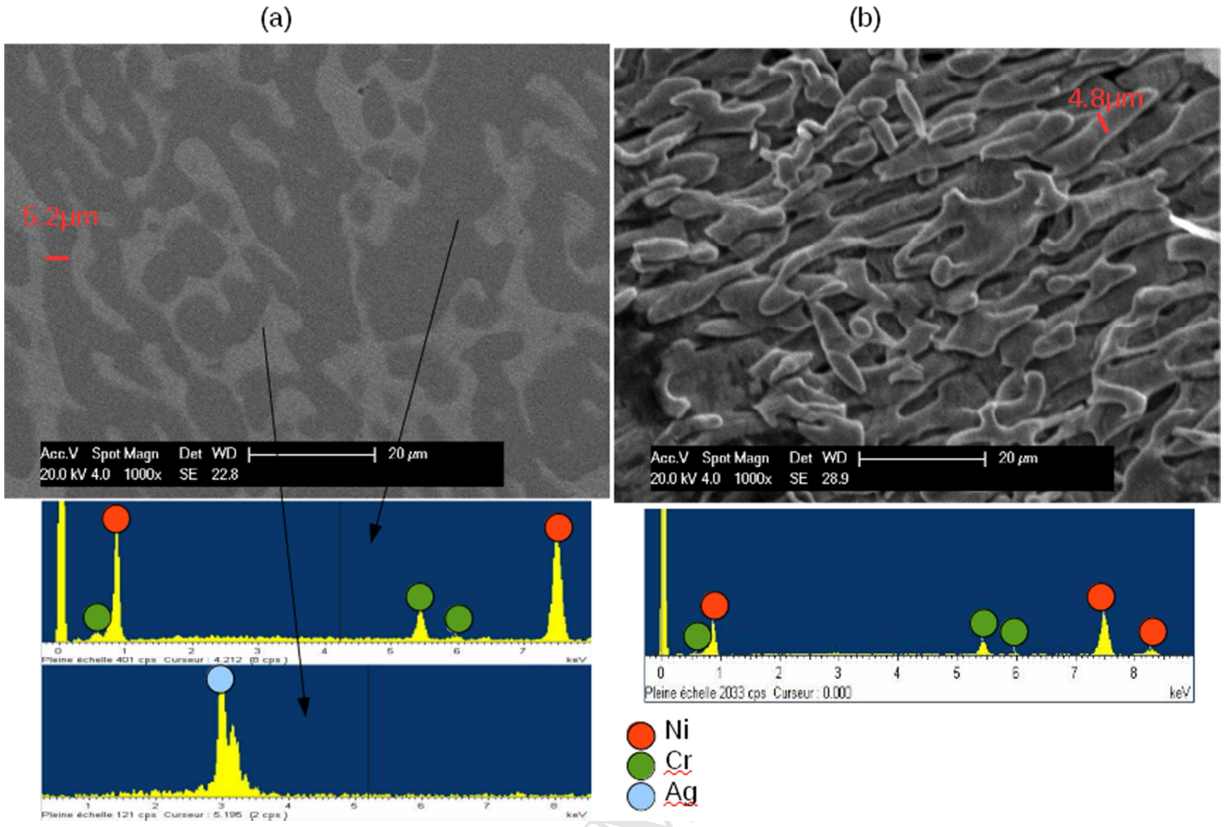

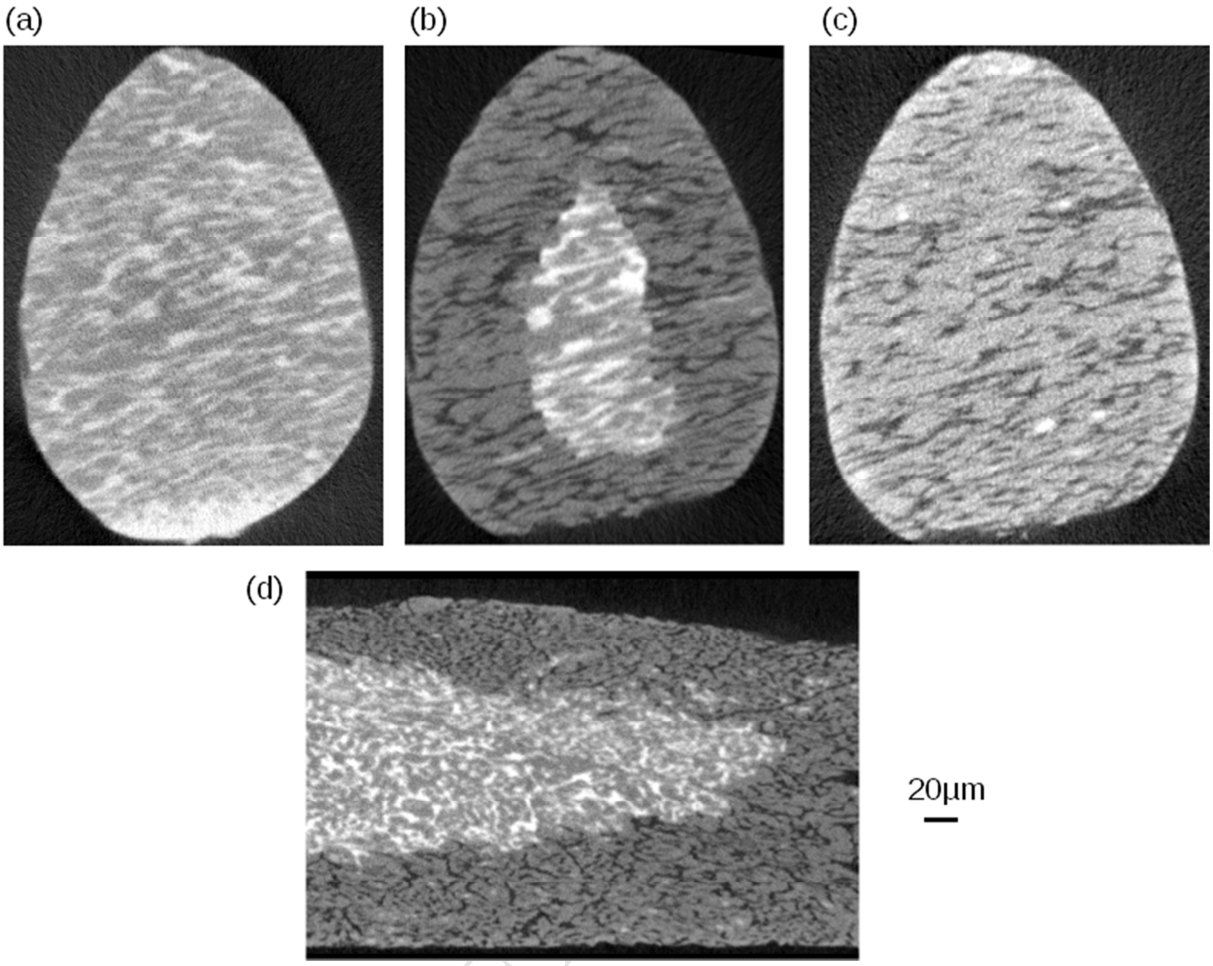

Highlights

→ *NiCr-Ag* composites were prepared by dealloying *Ni-Cr-Cu* precursor in an *Ag* melt bath
→ *NiCr-Ag* composites were cold-rolled to introduce anisotropy
→ The microstructure of *NiCr-Ag* composites and porous *NiC*r was studied using X-ray tomography
→ The mechanical properties of *NiCr-Ag* composites and porous *NiCr* were examined by nanoindentation